AIAA-92-5101
Hypersonic Turbulent Expansion-Corner Flow with Shock Impingement

K. Chung & F. Lu ,
University of Texas at Arlington,
Arlington, TX

AIAA FOURTH INTERNATIONAL AEROSPACE PLANES CONFERENCE
1 - 4 DECEMBER 1992/ORLANDO, FL

For permission to copy or republish, contact the
American Institute of Aeronautics and Astronautics
The Aerospace Center • 370 L'Enfant Promenade, SW • Washington, DC 20024-2518

HYPERSONIC TURBULENT EXPANSION-CORNER FLOW WITH SHOCK IMPINGEMENT

Kung-Ming Chung* and Frank K. Lu†
University of Texas at Arlington, Arlington, Texas, 76019-0018

Mean and fluctuating surface pressure data were obtained in a Mach 8, turbulent, cold flow past an expansion corner subjected to shock impingement. The expansion corner of 2.5 or 4.25 deg was located at 0.77 m (30.25 in.) from the leading edge of a sharp-edged flat plate while an external shock, generated by either a 2- or 4-deg sharp wedge, impinged at the corner, or at one boundary layer thickness ahead or behind the corner. The mean pressure distribution was strongly influenced by the mutual interaction between the shock and the expansion. For example, the upstream influence decreased when the shock impinged downstream of the corner. Also, the unsteadiness of the interactions was characterized by an intermittent region and a local rms pressure peak near the upstream influence line. The peak rms pressure fluctuations increased with a larger overall interaction strength. Shock impingement downstream of the corner resulted in lower peaks and also in a shorter region of reduced fluctuation levels. These features may be exploited in inlet design by impinging the cowl shock downstream of an expansion corner instead of at the corner. In addition, a limited Pitot pressure survey showed a thinning of the boundary layer downstream of the corner.

NOMENCLATURE

M	= Mach number
p	= pressure
pdf	= probability distribution function
U_τ	= friction velocity, $\sqrt{\tau_w/\rho_w}$
x	= distance measured from corner along test surface, Fig. 1
y	= distance normal to the test surface surface
Z	= standardized pdf variable, p'/σ_p
α	= corner angle, Fig. 1
δ	= boundary layer thickness
θ	= external wedge angle, Fig. 1
σ_p	= standard deviation of pressure fluctuations

Subscripts

e	= boundary layer edge
F	= inviscid conditions downstream of shock–expansion
$incip$	= incipient
max	= maximum in rms surface pressure distribution
o	= undisturbed boundary layer conditions at the corner location
pit	= Pitot
sh	= shock
U	= upstream influence
w	= mean wall value
1, 2, 2′, 3, 4	= inviscid regions, Fig. 1
∞	= incoming freestream or incoming static value

Superscripts

$()'$	= fluctuating value
$\overline{()}$	= normalized by δ_o

INTRODUCTION

Shock wave boundary-layer interactions have been the subject of considerable research.[1] Recently, renewed interest in supersonic and hypersonic flight vehicles has necessitated a better physical understanding of such interactions than previously achieved. One reason for this necessity is the increased accuracy required in designing these vehicles using computational methods. Unfortunately, complex shock boundary-layer interactions are amongst a number of flow phenomena which are barely understood at hypersonic Mach numbers.[2] The motivation of the present study is, therefore, to further the understanding of shock boundary-layer interactions through basic experimental research.

Specifically, the present study examines the hypersonic interaction that exists when a shock impinges near an expansion corner as depicted in Fig. 1. This is an idealized, building block interaction that models the impingement of a cowl shock near an expansion corner in an inlet at off-design conditions. Although the ulti-

*Graduate Research Associate, Aerodynamics Research Center, Mechanical and Aerospace Engineering Department. Student Member AIAA.

†Assistant Professor, Aerodynamics Research Center, Mechanical and Aerospace Engineering Department. Senior Member AIAA.

Copyright ©1992 by K.-M. Chung and F.K. Lu. Published by the American Institute of Aeronautics and Astronautics, Inc. with permission.

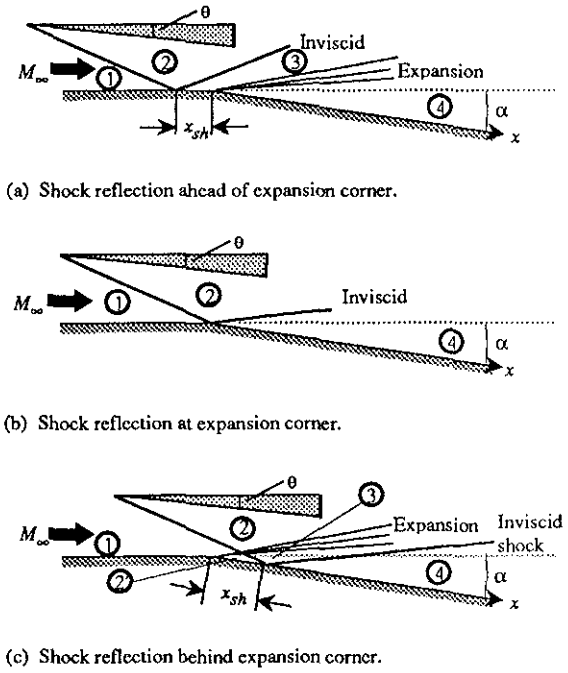

Figure 1: Schematic of test configurations.

mate goal is to support scramjet inlet design pertaining to hypersonic vehicles such as the National AeroSpace Plane, the present study is of a smaller scope because the shock–expansion interaction has been rarely studied. Hence, the present study involves small corner and wedge angles giving rise to unseparated interactions. Before discussing the results of the study, brief details of the experiment are outlined next.

EXPERIMENT

Shock Tunnel

The UTA shock tunnel is of conventional design and consists of a shock tube connected to a nozzle, test section, diffuser and dump tank. The driver section of the shock tube was connected to the driven section via a double-diaphragm section. Flow was initiated by rupturing the diaphragms which initially separated the driver and driven gases. The double-diaphragm arrangement provided precise control of the driver and driven pressures which in turn ensured repeatable stagnation conditions and unit Reynolds number.

A secondary diaphragm of thin Mylar® or aluminum foil was used to separate the driven tube and the nozzle. Once the secondary diaphragm was ruptured, the test gas in the driven tube was expanded by a conical nozzle with a 7.5-deg half-angle expansion to Mach 8 in a semi free-jet test section 0.54 m (21 in.) long and 0.44 m (12 in.) in diameter.

Test Model

A stainless steel, flat plate 203 mm (8 in.) wide by 0.96 m (37.75 in.) long with a sharp convex corner 768 mm (30.25 in.) from its leading edge was used to develop a boundary layer. Fences under the plate were used to prevent crossflows. In the test region, starting at about 750 mm (29.5 in.) from the flat-plate leading edge, the surface pressure without the corner showed an extremely slight, favorable longitudinal pressure gradient which can be ignored.[3] Within experimental accuracy, the undisturbed surface pressure was assumed uniform.

Two instrumentation plates with 2.5 and 4.25 ±0.1 deg expansion angles were fabricated for surface pressure measurements. Taps for flush-mounted transducers were drilled perpendicularly onto the test surface from 38.1 mm (1.5 in.) upstream to 60.3 mm (2.375 in.) downstream of the corner location. The taps were offset from the centerline by 3.18 mm (0.125 in.) and were spaced 6.35 mm (0.25 in.) or $0.5\delta_o$ apart.

An impinging shock was generated by a sharp wedge. This wedge consisted of a sharp-edged plate and an angle-of-attack adapter. The plate was made of aluminum and it was 130 mm (5.25 in.) long and 180 mm (7 in.) wide which enabled it to span the test region while its length ensured that expansion waves from the trailing edge impinged on the test surface downstream of the region of interest. The plate was tightened to an adapter to obtain the desired wedge angle of 2 or 4±0.1 deg. The wedge assembly was mounted to a sting and the shock impingement position was adjusted to be at the expansion corner, or one boundary layer thickness upstream and downstream of the corner as shown in Fig. 1. This figure also shows the inviscid wave pattern. Although Figs. 1b and c depict a reflected shock, other possibilities, depending on the values of α and θ, include a reflected expansion fan or a shock cancellation. Moreover, for consistency, the inviscid region downstream of the shock boundary-layer interaction is denoted as region 4 in Figs. 1a–c.

Data Acquisition and Instrumentation

For dynamic surface pressure measurements, Kulite Model XCS–093–5A and XCS–093–15A pressure transducers were flush mounted to be better than $0.005\delta_o$ in order to minimize interference with the flow.[4] Data from the pressure transducers were pre-conditioned by Leyh Model 29 amplifier and anti-aliasing filter combinations with a gain of 500 and a roll-off frequency of 100 kHz before being sent to two LeCroy Model 6810 four-channel, twelve-bit waveform recorders. Built-in programmable amplifiers were used to further condition the signals which were then digitized at 1 Megasamples/sec/channel and stored within the recorders. The

data were subsequently transferred to an Everex Step 286 host computer which also controlled the data acquisition system. The limited number of channels meant that a detailed pressure distribution was obtained through a number of runs.

The transducer models used have natural frequencies of 100 kHz and 150 kHz respectively as quoted by the manufacturer while the diameter of their sensing surfaces is 0.97 mm (0.038 in.). These characteristics have a bearing on the ability of the transducers to resolve pressure fluctuations. According to Corcos,[5] the maximum measurable frequency for transducers of this size in the present test conditions is about 280 kHz which cannot be attained due to the lower natural frequencies that these transducers possess. To obtain reliable dynamic data, the data were digitally filtered with a cutoff at 100 kHz before analysis was performed on them. Moreover, the limited spatial resolution of the present transducers resulted in these transducers capturing only 60 percent of the rms compared to an ideal transducer.[6] Further details on the resolution of surface pressure fluctuations in the present experiments can be found in Ref. 7.

Even though the transducers were used for dynamic measurements, a static calibration sufficed in determining the calibration coefficients.[8] In addition, the signal-to-noise ratio of the transducers was estimated to be about 20 dB (10:1) for $p < 0.3$ kPa (0.05 psia). However, the magnitude of the pressure signals increased substantially with shock impingement which consequently improved the signal-to-noise ratio to about 40 dB.[9]

Pitot pressure surveys were made with a boundary layer rake. The rake consisted of four Pitot probes with Kulite pressure transducers snuggled at 18 mm (0.7 in.) from the tip to ensure a fast response. The inside dimensions of the flattened intake were a height of 1.9 mm (0.075 in.) and a width of 0.25 mm (0.01 in.) high and the small height minimized displacement effects. A Pitot pressure profile was built up in about 4–5 runs.

Test Conditions

The tunnel was operated by first charging the driver tube and the double-diaphragm section to 24 MPa ± 1.5 percent (3,500 psia) and 12 MPa (1,750 psia) respectively. The driven tube was charged to 280 kPa (40 psia) ± 1.3 percent after being evacuated to remove moist ambient air. The nozzle, test section, diffuser and the dump tank were evacuated to less than 0.32 kPa (0.05 psia). The gas used throughout the tunnel was dried air. Breaking the two diaphragms by venting the double-diaphragm section started the tunnel whereby a shock propagated into the driven tube and an unsteady expansion wave propagated into the driver tube. The shock Mach number M_s was found to be 2.15 with a run-to-run variation of less than ±5 percent; the low shock Mach number ensured that real gas effects were negligibly small. From the shock Mach number and the initial driver and driven conditions, the stagnation pressure and temperature were estimated as 5.38 MPa (780 psia) and 800 K (1 440 °R) respectively while the unit Reynolds number was estimated as $10.2 \times 10^6\,\mathrm{m}^{-1}$ (3.1×10^6/ft). The flat plate was at room temperature ($T_w \approx 290$ K, 522 °R) and thus the experiments were performed under cold-wall conditions ($T_w/T_o \approx 0.35$). Further, the undisturbed boundary layer developed naturally on the flat plate and the boundary layer thickness at the corner location was determined to be 12.7 ± 2 mm (0.50 ± 0.08 in.).[3] Through the test region, the low Reynolds number of 1 800–2 300 based on the momentum thickness produced a turbulent boundary layer with a negligible wake in the test region. Finally, the useful test time was about 0.5 ms and it provided the lower cutoff frequency to the test data of about 2 kHz.

RESULTS AND DISCUSSION

Mean Surface Pressure

Surface pressures are normalized by the incoming freestream static pressure p_∞ and are plotted in Figs. 2 and 3 respectively. In each figure, the surface pressure distribution for the three shock impingement locations of $\bar{x}_{sh} \equiv x_{sh}/\delta_o = -1$, 0 and 1 are presented. The inviscid pressure distributions are also shown as solid lines.

With the incident shock upstream of the expansion corner, Figs. 2a and 3a show that the surface pressure gradually increases from the upstream influence of the shock but it does not reach the downstream, inviscid, reflected shock value p_3/p_1, see Fig. 1 for inviscid flow nomenclature. Unlike shock reflection off a flat surface, the close proximity of the expansion corner prevents the surface pressure from attaining the downstream inviscid shock value. Moreover, the surface pressure maxima is reduced with a stronger expansion. For example, for $\theta = 4$ deg, the peak pressure $p_{pk}/p_\infty \approx 3.4$ when $\alpha = 2.5$ deg but is only 2.6 when $\alpha = 4.25$ deg. This implies that the expansion corner serves to attenuate the pressure rise that would otherwise occur. For a given incoming shock, the attenuation depends on the overall interaction strength characterized by p_F/p_1.

Downstream of the expansion corner, the surface pressure tends to the inviscid value. A corner "downstream influence" x_D can be defined as the intercept between the slope of the downstream pressure distribution and the downstream inviscid value.[10] Although the downstream influence is difficult to determine due to the gentle pressure gradient, it is of the order of 1–$2\delta_o$. This is shorter than that of a pure, expansion corner in which $\bar{x}_D \approx 5$–6 for the same test conditions.[10]

Thus, the downstream influence decreases with increasing p_F/p_1.

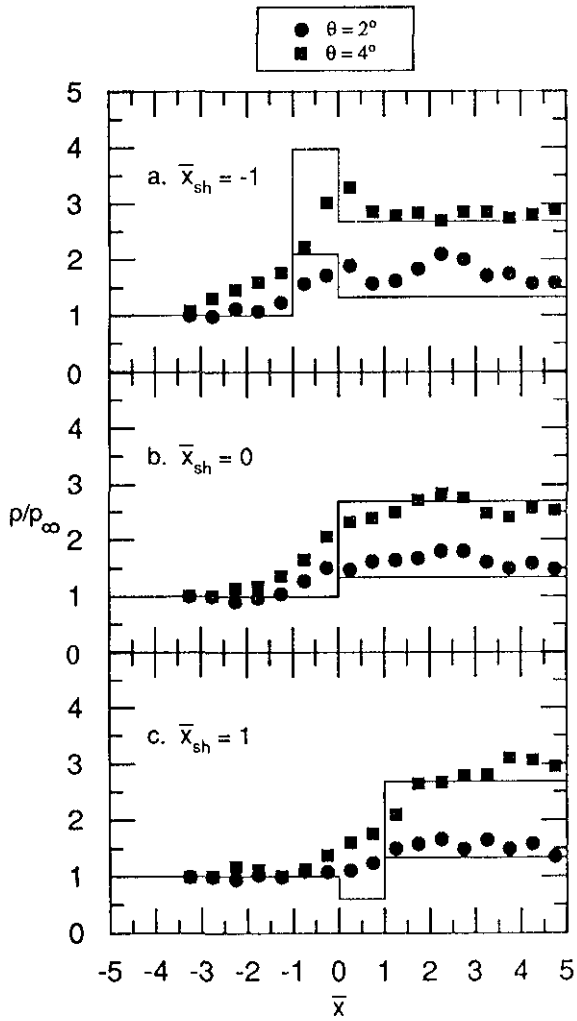

Figure 2: Shock impingement near 2.5-deg expansion corner.

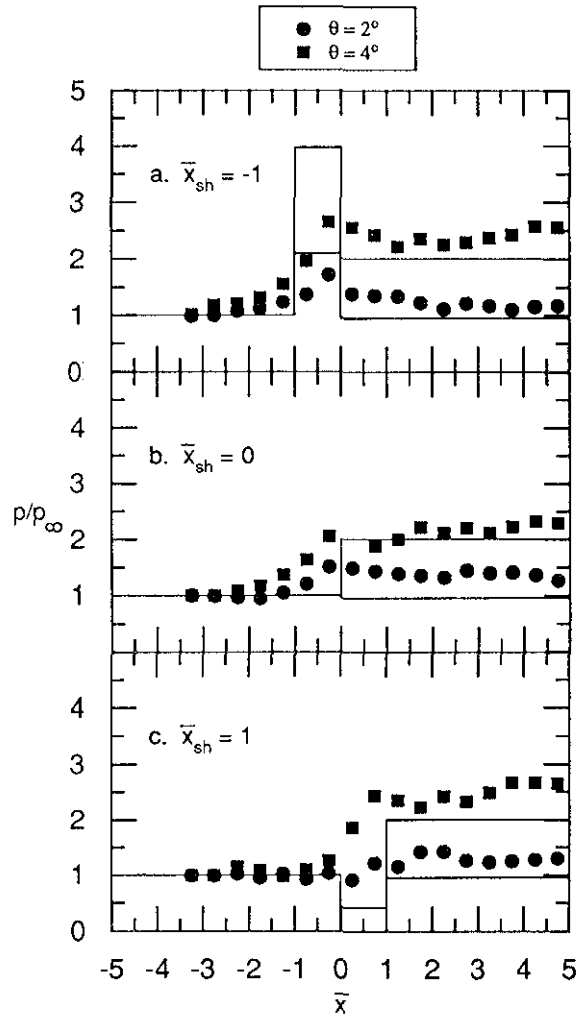

Figure 3: Shock impingement near 4.25-deg expansion corner.

The upstream surface pressure distribution when the shock impinges right at the corner appears similar to that when the shock impinges ahead of the corner except for a small reduction in upstream influence, compare Figs. 2b and 3b with Figs. 2a and 3a. (This will be elaborated later.) Under certain conditions in which $p_F/p_1 \approx 1$, the reflected shock wave at the corner is nearly "neutralized" by the Prandtl-Meyer expansion, as observed previously by Chew.[11]

When the shock impinges downstream of the corner, Figs. 2c and 3c, the surface pressure distribution shows a smaller upstream influence as compared to the other configurations. This decrease in the upstream influence shows that the expansion corner plays an important role in the shock boundary-layer interaction through modifying the incoming boundary layer characteristics. According to Elfstrom,[12] the upstream propagation of pressure at incipient separation depends on the incom-

ing Mach number and on the Reynolds number based on wall conditions $Re_w = U_\tau \delta / \nu_w$. The upstream influence decreases with an increase in Re_w and this behavior may be expected to hold for attached interactions as well. For small expansion corners in hypersonic, high Reynolds number flow, the friction velocity and the dynamic viscosity at the wall do not differ greatly from incoming values.[13] However, the expansion produces a thickening of the boundary layer[9] and thereby an increase in Re_w. Consequently, the upstream influence is decreased based on Elfstrom's analysis.

Figs. 2c and 3c also show that although the inviscid pressure distribution consists of a pressure drop followed by a pressure rise, the actual pressure distribution for all four cases does not show any significant pressure decrease due to the expansion. This is unlike Chew's observation[11] in a supersonic flow in which the separate effects of the shock and expansion fan can be distinguished clearly when these waves were separated by about 1.5–2.5δ_o. In a hypersonic flow, the surface pressure decreases in a more uniform fashion due to the highly-swept expansion fan. The separate wave structure due to the expansion and the shock in a hypersonic flow may perhaps be achieved only when the shock impinges upon the corner further downstream.

The surface pressure with a 4.25-deg expansion for both impinging shocks shows an overshoot compared with inviscid pressure levels.[11] The pressure distributions arising from the same shocks impinging a flat plate[9] or the weaker expansion corner, however, do not exhibit the overshoot. This overshoot appears to be a unique feature arising from the mutual interactions of the incident shock and the expansion fan. The suggestion that the overshoot is due to three-dimensional effects arising from tunnel side-wall interactions does not appear feasible in the present unseparated interactions.[11] No explanations, unfortunately, are forthcoming at the moment for this phenomenon.

To quantify the above observations on the upstream influence, the normalized upstream influence $\bar{x}_u \equiv \bar{x}/\delta_o$ is plotted against $\bar{x}_{sh}$ in Fig. 4. The upstream influence is larger for a higher shock strength as expected. For the same shock strength, when the shock impinges downstream, the upstream influence decreases. The decrease of upstream influence for the weaker incident shock is, however, extremely slight. The expansion corner affects the upstream influence in two ways. First is the proximity of the corner; as the shock impinges from ahead to behind the corner, the upstream influence decreases. Secondly, the stronger the expansion, the smaller the upstream influence.

Surface Pressure Fluctuations

The rms distribution of pressure fluctuations are shown in Figs. 5 and 6. The rms distribution of pressure fluctuations σ_p is normalized by the local surface pressure

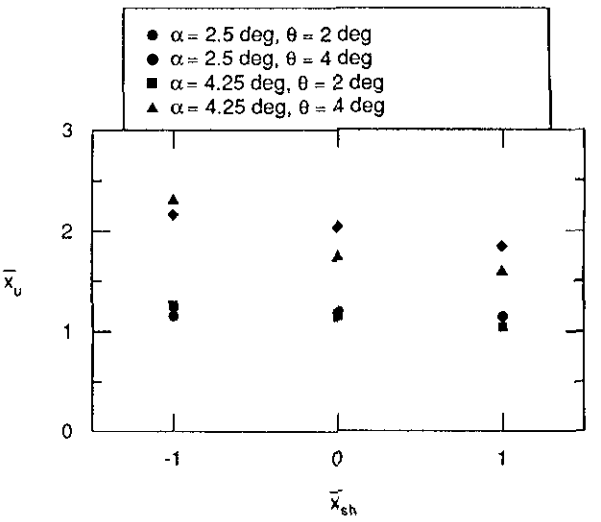

Figure 4: Upstream influence due to shock impingement near expansion corners.

p. The normalized rms distribution with shock impingment at $\bar{x}_{sh} = -1$ show some similiar features with one another, e.g., the "peak" rms pressure fluctuation associated with the strong intermittent behavior of the interaction, a damping downstream of the expansion corner and an increase at $\bar{x} = 3.3$–4.2. This downstream increase of the surface pressure fluctuations may be due to a change of the boundary layer state, from one that is "relaminarizing" due to the favorable pressure gradient to one that is "retransitioning" as the boundary layer re-develops to a new equilibrium turbulent state. The downstream peak in σ_p also appears related to the downstream peak in mean pressure.

When the shock impinges right at the expansion corner, the characteristic shape of the rms pressure distribution is basically the same as that of shock impingement upstream of the expansion corner. However, the "neutralization" of the shock by the expansion fan reduces the rms peak. For $\alpha = 4.25$ deg and $\theta = 2$ deg, $(\sigma_p/p)_{max}$ is about 20 percent below the peak value achieved when the shock impinges upstream of the corner. The rms pressure distribution when the shock impinges downstream of the corner shows the effect of the expansion in attenuating the peak rms value and, further, results in a more severe damping of the fluctuations throughout the downstream region.

The peak rms value $(\sigma_p/p)_{max}$ is plotted against $\bar{x}_{sh}$ in Fig. 7. The figure shows that the peak rms value decreases as the impinging shock moves downstream. This feature, in addition to the lower mean pressure levels, may be exploited in inlet design where the cowl shock is allowed to impinge downstream of an expansion corner under on-design conditions. Also, the peak rms values for the 4.25-deg expansion for both wedge angles appear to be more attenuated compared with those of

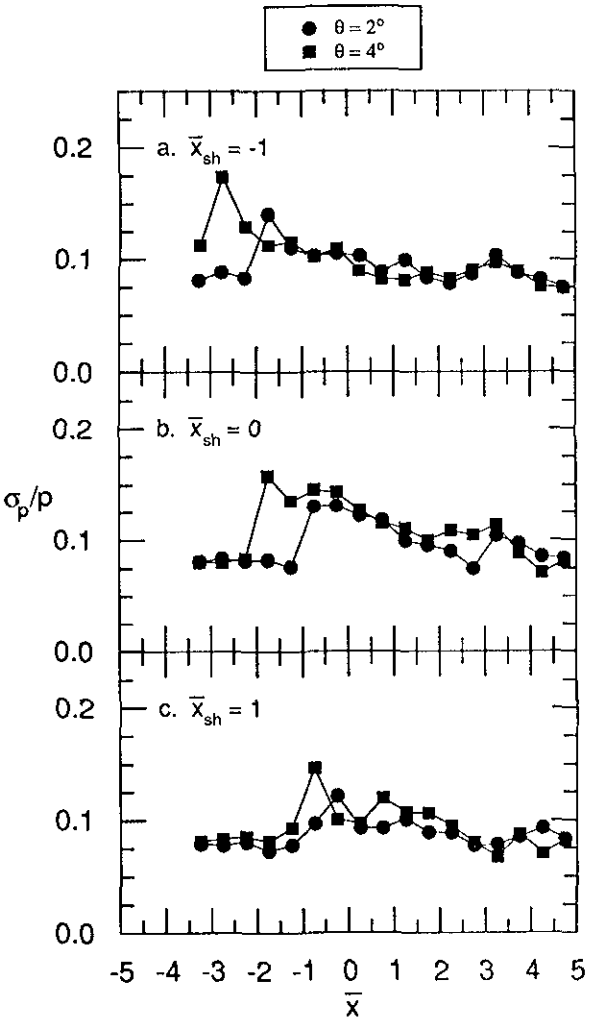

Figure 5: Root-mean-square pressure distribution due to shock impingement near 2.5-deg expansion corner.

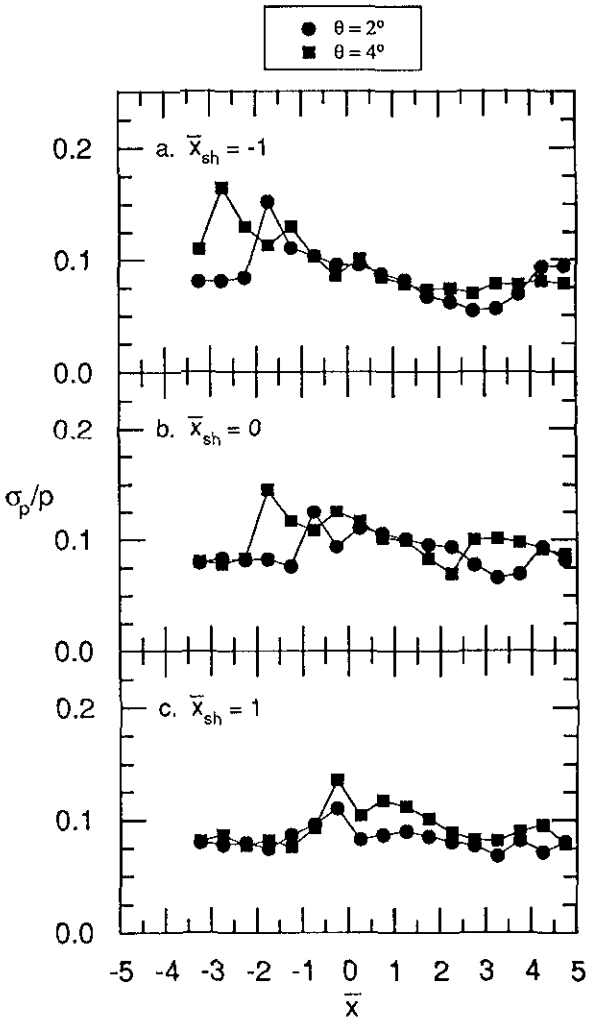

Figure 6: Root-mean-square pressure distribution due to shock impingement near 4.25-deg expansion corner.

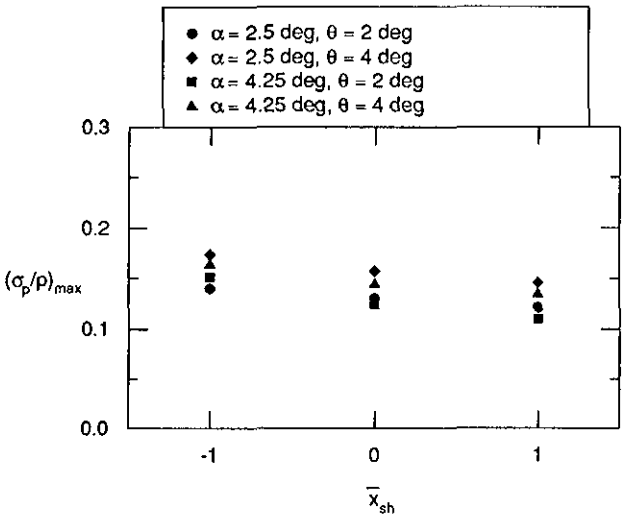

Figure 7: Peak values of rms pressure.

the 2.5-deg expansion which reveals the influence of expansion corner on the surface pressure fluctuations.

The increase in surface pressure fluctuations is thought to be due to shock motion[14] and can be further understood through examining the probability density functions. Examples of pdfs normalized by the mean local pressure are plotted in Figs. 8 and 9 against the normalized coordinate $Z = p'/\sigma_p$. The normalized Gaussian distribution is plotted as a solid line in these figures. The pdfs show a departure from the Gaussian downstream of the interaction onset in which a highly skewed distribution is obtained followed by a bimodal one. These features indicate the presence of an intermittent pressure distribution in which the pressure "switches" from an upstream, lower value, to a downstream, higher value.[14] Also, a comparison of Figs. 8 and 9 reveals that the upstream propagation of disturbances due to the 4-deg wedge is further than that due to the 2-deg wedge. Thus the pdfs show a larger upstream influence due to the stronger shock interaction.

Pitot Pressure Surveys

Pitot pressure surveys were performed for only two test conditions, namely, where the oblique shock impinges at the 2.5-deg expansion corner. The inviscid solution provides for a shock reflection in both cases. The Pitot pressure, normalized by the value at the boundary layer edge $p_{pit,e}$, are plotted against the perpendicular distance from the wall, normalized by the local boundary layer thickness, in Fig. 10. The profiles were obtained from $\bar{x} = 0.75$–2.75 (4.8–35 mm or 0.375–1.375 in.) downstream of the corner. The profiles for both wedge angles show a fairly similiar shape. A distortion, whose limits are indicated by a pair of arrowheads in the first profile of Fig. 10a, is observed. This distortion, which is associated with reflected compression waves, is smeared through the boundary layer and is less distinct compared with those found in Pitot surveys of flat plate flow with shock impingement.[9,15]

Further, the boundary layer thickness extracted from the Pitot pressure profiles is shown in Fig. 10. The boundary layer thickness decreases downstream of the corner. For flow past an expansion corner only, the boundary layer thickens more rapidly than that past a flat plate.[9] The more rapid increase is due to a reduction of density through the expansion fan.[16] However, when a shock impinges on the corner, the downstream boundary layer thickness is reduced. This resembles that of a weak shock impinging a flat plate.[1]

CONCLUSIONS

A complicated interaction exists when a shock impinges near an expansion corner. The favorable pressure gradient set up by the expansion, e.g., attenuates the upstream influence and limits the surface pressure from reaching the downstream inviscid shock value. The expansion also reduces the unsteadiness inherent in shock, turbulent boundary-layer interactions, including unseparated ones. Moreover, even when the mean surface pressure shows shock cancellation by the expansion fan, a peak still exists in the rms distribution. It appears that the expansion corner has the largest effect on the shock boundary-layer interaction if the shock impinges behind the corner. Finally, the shock is reflected at a shallow angle and remains embedded within the boundary layer even at $3\delta_o$ from the corner.

ACKNOWLEDGEMENTS

The research was supported by NASA Langley Grant NAG 1-891 monitored by Dr. J.P. Weidner. This support is gratefully acknowledged. The authors also thank Messrs. Gene Sloan and Jim Holland for technical assistance in performing the experiments.

REFERENCES

1. Délery, J. and Marvin, J.G., "Shock-Wave Boundary Layer Interactions," AGARDograph No. 280, 1986.

2. Marvin, J.G., "CFD Validation Experiments for Hypersonic Flows," AIAA Paper 92-4024, July 1992.

3. Chung, K.-M. and Lu, F.K., "An Experimental Study of a Cold-Wall Hypersonic Boundary Layer," AIAA Paper 92-0312, January 1992.

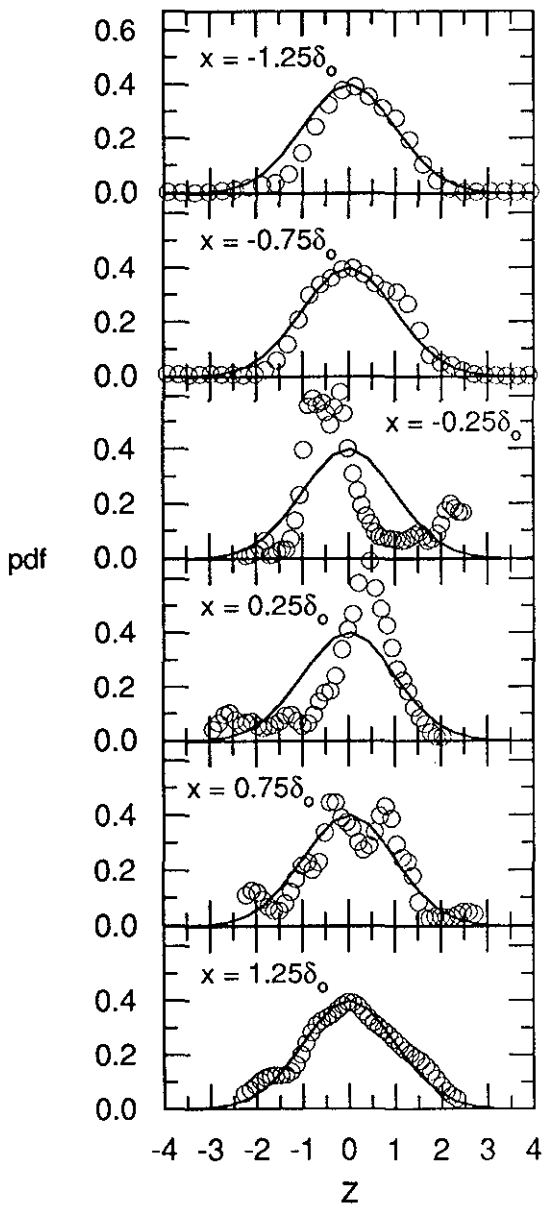

Figure 8: Probability distribution functions of shock impingement downstream of 2.5-deg expansion ($\theta = 2$ deg, $\bar{x}_{sh} = 1$).

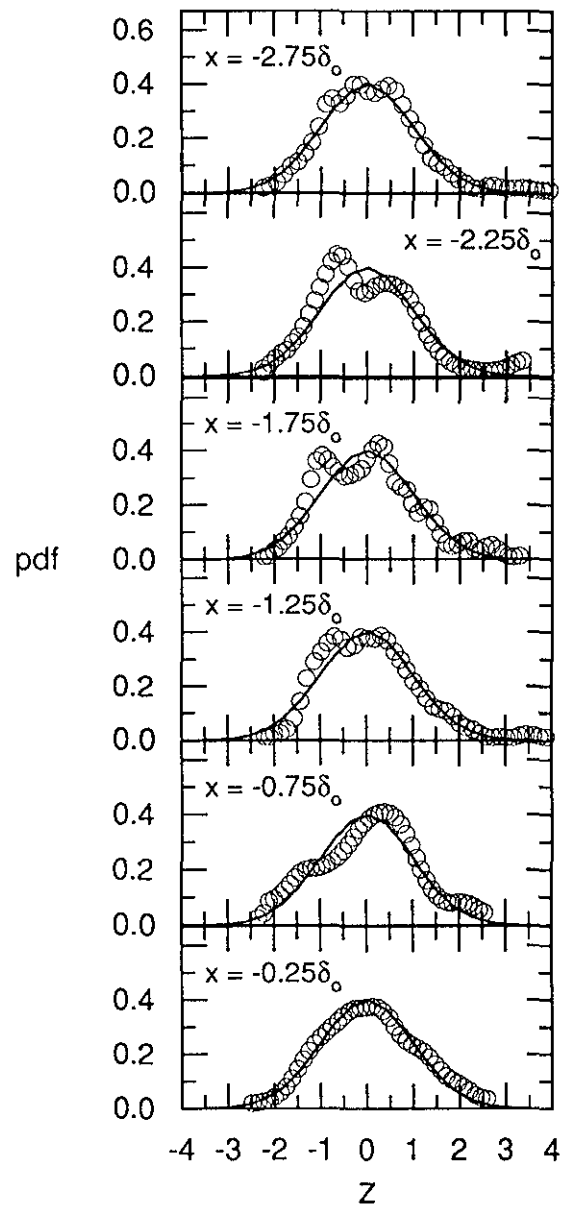

Figure 9: Probability distribution functions of shock impingement downstream of 2.5-deg expansion ($\theta = 4$ deg, $\bar{x}_{sh} = 1$).

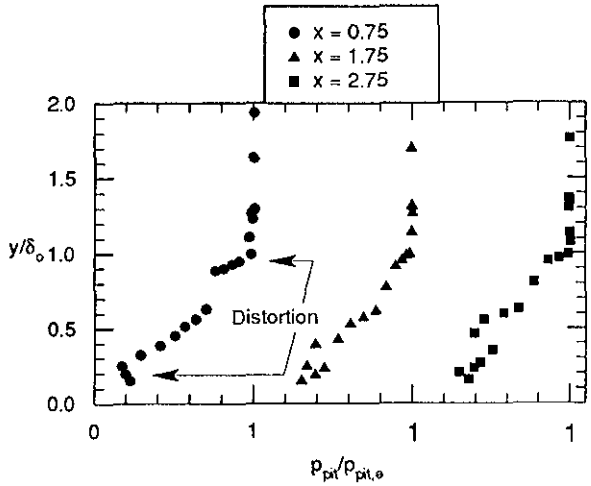

a. $\alpha = 2.5$ deg, $\theta = 2$ deg.

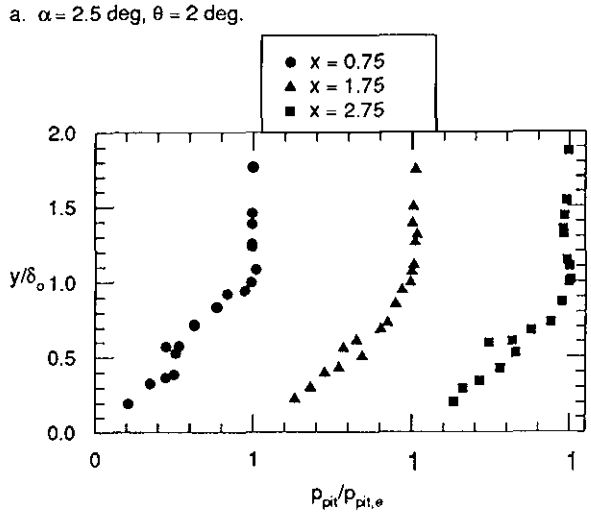

b. $\alpha = 2.5$ deg, $\theta = 4$ deg.

Figure 10: Pitot pressure profiles for shock impingement on 2.5-deg expansion corner.

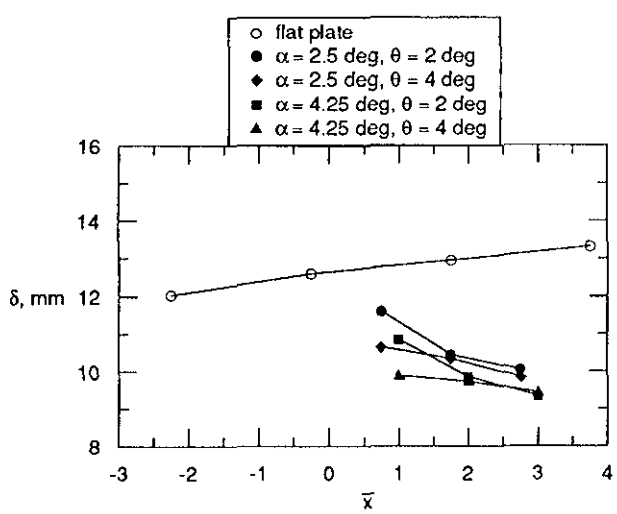

Figure 11: Boundary layer thickness due to shock impingement at an expansion corner.

4. Coe, C.F., "Surface-Pressure Fluctuations Associated With Aerodynamic Noise," NASA SP–204, 1956, pp. 409–424.

5. Corcos, G.M., "Resolution of Pressure in Turbulence," *Journal of the Acoustical Society of America*, Vol. 35, No. 2, 1963, pp. 192–199.

6. Schewe, G., "On the Structure and Resolution of Wall-Pressure Fluctuations Associated with Turbulent Boundary Layer Flow," *Journal of Fluid Mechanics*, Vol. 134, 1983, pp. 311–328.

7. Chung, K.-M. and Lu, F.K., "Damping of Surface Pressure Fluctuations in Hypersonic Turbulent Flow Past Expansion Corners," *AIAA Journal*, in press 1993.

8. Chung, K.-M. and Lu, F.K., "Shock Tube Calibration of a Fast-Response Pressure Transducer," AIAA Paper 90–1399, June 1990.

9. Chung, K.-M., "Shock Impingement Near Mild Hypersonic Expansion Corners," Ph.D. Dissertation, University of Texas at Arlington, December 1992.

10. Lu, F.K. and Chung, K.-M., "Downstream Influence Scaling of Turbulent Flow," *AIAA Journal*, in press 1992.

11. Chew, Y.T., "Shock Wave and Boundary Layer Interactionn in the Presence of an Expansion Corner," *Aeronautical Quarterly*, Vol. XXX, 1979, pp. 506–527.

12. Elfstrom, G.M., "Turbulent Hypersonic Flow at a Wedge-Compression Corner," *Journal of Fluid Mechanics*, Vol. 53, Part 1, 1972, pp. 113–127.

13. Adamson, T.C., "Effect of Transport Properties on Supersonic Expansion around a Corner," *Physics of Fluids*, Vol. 10, No. 5, 1967, pp. 953–962.

14. Dolling, D.S. and Or, C.T., "Unsteadiness of the Shock Wave Structure in Attached and Separated Compression Ramp Flows," *Experiments in Fluids*, Vol. 3, 1985, pp. 24–32.

15. Green, J.E., "Reflexion of an Oblique Shock Wave by a Turbulent Boundary Layer," *Journal of Fluid Mechanics*, Vol. 40, Part 1, 1970, pp. 81–95.

16. Chew, Y.T. and Squire, L.C., "The Boundary Layer Development Downstream of a Shock Interaction at an Expansion Corner," British Aeronautical Research Council Reports and Memoranda No. 3839, August 1978.